PNAS

Supporting Information for

Disruption of constitutive CXCR4 oligomers impairs oncogenic properties in lymphoid neoplasms

Simon Mobach, Nick D. Bergkamp, Ziliang Ma, Marco V. Haselager, Stephanie M. Anbuhl, Daphne Jurriens, Jelle van den Bor, Ziming Wang, Caitrin Crudden, Jamie L. Roos, Claudia V. Perez Almeria, Rick A. Boergonje, Martin J. Lohse, Reggie Bosma, Eric Eldering, Marco Siderius, Wei Wu, Marcel Spaargaren, Sanne H. Tonino, Arnon P. Kater, Martine J. Smit* & Raimond Heukers*

* Corresponding authors: Martine J. Smit and Raimond Heukers
Email: mj.smit@vu.nl and r.heukers@vu.nl

This PDF file includes:

Detailed Materials and Methods

DNA constructs and molecular cloning

The pcDEF3 vector was a gift from Langer (*1*). cDNA encoding the BRET-based cAMP biosensor His-CAMYEL pcDNA3.1(L) was purchased from ATCC (#ATCC-MBA-277). pLKO.1 puro CXCR4 siRNA-1 and siRNA-2 were gifts from Bob Weinberg (Addgene plasmids #12271 and #12272). plKO.1 scramble shRNA was a gift from David Sabatini (Addgene plasmid #1864). Myc-CXCR4-Rluc pIRES, HA-CXCR4-YFP pIRES (*2*), HA-CXCR4 WT pcDEF3 (*3*), HA-CXCR4-N119S pcDEF3 (19), NanoLuc-CXCR4 pcDNA3.1 (*4*) and CXCR4-EYFP pcDNA3 (*5*) were described previously. HA-CXCR4 pLenti6.3/TO/V5-DEST was generated by exchanging US28 for CXCR4 in the previously described HA-US28 pLenti6.3/TO/V5-DEST plasmid (*6, 7*). HA-CXCR4 pEUI was generated by exchanging VUN103-FLAG for HA-CXCR4 in the previously described VUN103-FLAG pEUI plasmid (*8*).

Patient material

After written informed consent, patient blood samples were obtained during diagnostic or follow-up procedures at the Departments of Hematology and Pathology of the Academic Medical Center Amsterdam. This study was approved by the AMC Ethical Review Biobank Board under the number METC 2013/159 and conducted in accordance with the Declaration of Helsinki. Peripheral blood mononuclear cells (PBMCs) of patients with CLL, obtained after Ficoll density gradient centrifugation (Pharmacia Biotech), were cryopreserved and stored as previously described (*9*). On the day of the experiment, the PBMCs were thawed in a water bath at 37°C. Thawing medium, consisting of Iscove's Modified Dulbecco's Medium (IMDM, Gibco) supplemented with 100 units of penicillin, 100 g/mL streptomycin (P/S, Gibco) and 20% (v/v) Fetal Bovine Serum (FBS, Bodinco), was added and cells were rested in the dark for 20 min at RT. Next, the thawing medium was removed, and cells were washed by centrifuging for 5 min at 300 x g with the deacceleration rate set at 7. Cells were then resuspended in assay buffer, consisting of IMDM supplemented with 10% FBS and 1% P/S. Cells were counted, and a viability of ≥ 70% was ensured by conducting a trypan blue staining using a LUNA-II™ automated brightfield cell counter (Logos Biosystems).

Cell lines and cell culture

Human embryonic kidney 293T (HEK293T) and CHO-K1 cells were obtained from American Type Culture Collection (ATCC). MEC-1, PGA-1, L363, CCRF-CEM, Jeko-1, CII, Namalwa, Maver-1 and Z-138 were described previously (*10*). RPCI-WM1 and TMD8 were kindly provided to Marcel Spaargaren by Dr. S.P. Treon and Dr. G. Lenz, respectively. HEK293T cells were cultured in Dulbecco's Modified Eagle's Medium (DMEM, Gibco) supplemented with 10% FBS and 1% P/S. CHO-K1 cells were cultured in DMEM/F-12, supplemented with 10% FBS and 1% P/S. MEC-1, RPCI-WM1, TMD-8, PGA-1, L363, CCRF-CEM, Jeko-1, CII, Namalwa, Maver-1 and Z-138 cells were cultured in IMDM supplemented with 10% FBS and 1% P/S. One day prior to experiments, suspension cells were prepared at a concentration of 1×10^6 cells/mL, and adherent cells were maintained in culture under non-confluent conditions. On the day of the experiment, cells were counted, and viability of ≥ 90% was ensured by conducting a trypan blue staining using a LUNA-II™ automated brightfield cell counter.

Nanobody generation and production

Previously described nanobodies were cloned into the pMEK222 bacterial expression vector with a C-terminal FLAG-6xHis tag (*11-13*). VUN415-NanoLuciferase (VUN415-NanoLuc) and VUN416-NanoLuc were generated by subcloning VUN415 and VUN416 into a modified version of the pMEK222 vector, with a C-terminal upper Hinge linker–NanoLuciferase–6xHis tag (*14*). BL21 Codon+ bacteria transformed with these pMEK222 plasmids were grown O/N in 10 mL of 2xYT medium, supplemented with glucose (2%) and ampicillin (1 µg/mL). The next day, this O/N culture was inoculated (1:100) in Terrific Broth with ampicillin (1 µg/mL). After bacteria grew at 37 °C to an OD_{600} of 0.5, nanobody production was initiated by adding isopropyl β-D-1-thiogalactopyranoside (1 mM), and incubation took place for 4 h at 37 °C. After centrifugation, pellets were frozen O/N at -20 °C. After thawing and dissolving the pellet in phosphate-buffered saline (PBS, pH 7.4), periplasmic extracts were incubated head-over-head for 1.5 h at 4 °C. Nanobodies were purified from the periplasm using immobilized affinity chromatography (IMAC) via 6x-His tags. Nanobodies bound to ROTI®-Garose cobalt agarose beads (Carl Roth) were eluted with 150 mM imidazole (Sigma-Aldrich). Afterwards, the buffer of nanobody

eluates was exchanged for PBS by O/N dialysis using Snakeskin Dialysis Tubing (Thermo Fisher Scientific). Dialyzed fractions were combined and stored at -20 °C until experiments.

Fluorescent labeling of nanobodies

The labeling of CXCR4 nanobodies with ATTO565 fluorescent dyes (ATTO-TEC, #AD565-41, #AD565-31) using thiol-maleimide coupling and N-hydroxy-succinimide (NHS) chemistry was described previously (*4*). Nanobodies containing an unpaired cysteine in the C-terminal tag used for fluorophore thiol-maleimide conjugation were provided by QVQ (Utrecht, the Netherlands). UV-VIS spectrometry was performed to ensure a degree of labeling (DOL) > 0.5. Free dye of <5% was assessed by SDS-PAGE, followed by a fluorescence scan using an Odyssey imager (LI-COR, at suboptimal wavelength to prevent detector saturation) or Azure400 imager (Azure Biosystems, at 524 nm excitation). In a similar fashion, VUN415-Cys was conjugated using thiol-maleimide coupling with an excess of Alexa Fluor 647 C2-maleimide (Invitrogen, A20347), to ensure a DOL of 1.

Transfection of HEK293T cells

HEK293T cells were transfected with a total of 1 µg DNA and 6 µg 25 kDa linear polyethyleneimine (PEI, Polysciences Inc.) in 150 mM NaCl solution per 1×10^6 cells. DNA encoding receptors and biosensors was, if necessary, supplemented with empty pcDEF3 to obtain a total DNA amount of 1 µg. The DNA-PEI mixture was vortexed for 3 s and incubated for 15 min at room temperature (RT). HEK293T cells were detached with Trypsin (Gibco) and resuspended in DMEM. The HEK293T cell suspension was added to the DNA-PEI mixture, and cells were seeded at 3.5×10^4 per well in white flat-bottom 96-well plates (Greiner Bio-One).

Receptor oligomerization CXCR4-Rluc and CXCR4-YFP

For receptor oligomerization experiments using tagged receptors, HEK293T cells were transfected with 40 ng Myc-CXCR4-Rluc and 400 ng HA-CXCR4-YFP. After 48 h incubation, cells were washed once using PBS and maintained in Hank's Buffered Saline Solution (HBSS), supplemented with 0.1% BSA, 1 mM $MgCl_2$, and 2 mM $CaCl_2$. Cells were stimulated with increasing concentrations of CXCL12, small

molecules, or nanobodies for 15 min before BRET measurements. After incubating cells for 10 min with 5 µM coelenterazine-h substrate (Promega), bioluminescence was measured at 535/30 nm and 475/30 nm using a PHERAstar plate reader (BMG). BRET signals were determined by dividing the ratio of luminescence in the acceptor channel by the donor channel. The ligand-promoted BRET signal was calculated by dividing the pre-read-normalized BRET values of each ligand concentration by the BRET ratio obtained for the vehicle condition.

CAMYEL constitutively active CXCR4

To assess potential inverse agonism of ligands on basal $G\alpha_{i/o}$ activation, HEK293T cells were transfected with 500 ng constitutively active CXCR4 mutant (HA-CXCR4 N119S) and 500 ng CAMYEL. After 48 h incubation, cells were washed once using PBS and maintained in HBSS, supplemented with 0.1% BSA, 1 mM $MgCl_2$, and 2 mM $CaCl_2$. After 20 min stimulation with 100 nM CXCL12, 10 µM small molecules, 1 µM VUN415, and 15 min stimulation with 1 µM forskolin (i.e., adenylyl cyclase activator), BRET measurements were performed. After incubating cells for 10 min with 5 µM coelenterazine-h substrate, bioluminescence was measured at 535/30 nm and 475/30 nm using a PHERAstar plate reader.

Oligomer detection using nanobody-based BRET in transfected HEK293T cells

To detect nanobody-based oligomerization BRET, HEK293T cells were transfected with 500 ng HA-CXCR4 pcDEF3 or HA-CXCR4 pEUI. For FKBP experiments, HEK293T cells were transfected with 2 ng HA-CXCR4 or 2 ng HA-CXCR4-FKBP. For HA-CXCR4 pEUI, increasing concentrations of tebufenozide (Sigma-Aldrich) were added to the culture medium 6 h post-transfection. After 48 h, cells were washed once with PBS. In the case of FKBP experiments, cells were treated with or without 1 µM AP20187 for 1 h. Subsequently, increasing equimolar concentrations of VUN415-NanoLuc and VUN415-ATTO565 or a constant concentration of detection nanobodies (31.6 nM) with different donor to acceptor ratios in assay buffer (HBSS, supplemented with 0.1% BSA, 1 mM $MgCl_2$, and 2 mM $CaCl_2$) were added to the cells. After incubation for 2 h at RT, cells were washed twice with PBS, and assay buffer was added. Subsequently, fluorescence of fluorescently labeled nanobodies was measured using

a CLARIOstar plate reader at 563/30 nm excitation and 592/30 nm emission. After the addition of 15 µM furimazine substrate (NanoGlo Luciferase Assay System, Promega), luminescence was measured using a PHERAstar plate reader with 610 nm/LP and 460/80 nm filters until the luminescence signal stabilized.

ELISA for surface expression of ecdysone-inducible CXCR4

In parallel with the BRET experiment described before, 3.5×10^4 transfected HEK293T cells were seeded in a transparent flat-bottom 96-well plate (Greiner Bio-One). Increasing concentrations of tebufenozide were added to the culture medium 6 h post-transfection. After 48 h, cells were fixed using 4% paraformaldehyde (PFA) in PBS, and plates were washed with PBS. Subsequently, blocking was performed with 2% (w/v) skimmed milk in PBS for 1 h at RT. Antibody incubations were also performed using this blocking buffer. CXCR4 expression was detected with the monoclonal mouse anti-CXCR4 antibody 12G5 (1:1000, Thermo Fisher Scientific, #35-8800) and horseradish peroxidase (HRP)-conjugated goat-anti-mouse antibody (1:2000, Bio-Rad, #1706516). Incubations with these antibodies were performed for 1 h at RT. Wells were washed three times with PBS between all incubation steps. Binding was determined with 1-step Ultra TMB-ELISA substrate (Thermo Fisher Scientific), and the reaction was stopped with 1M H_2SO_4. Optical density was measured at 450 nm using a CLARIOstar plate reader.

Membrane extract preparation

Two million HEK293T cells were plated in a 10 cm^2 dish (Greiner Bio-One). The next day, cells were transfected with 250 ng NanoLuc-CXCR4, supplemented to a total of 5 µg DNA with empty pcDEF3 vector, and 30 µg PEI in 150 mM NaCl solution. The DNA-PEI mixture was vortexed for 3 s and incubated for 15 min at RT. Subsequently, the mixture was added dropwise to the adherent HEK293T cells. Protein expression was allowed to proceed for 48 h. The media was then removed, and the cells were washed once with cold PBS. Next, cells were detached and resuspended in cold PBS. Cells were centrifuged at 1500 × *g* at 4 °C, resuspended in cold PBS, and again centrifuged at 1500 × *g* at 4 °C. The pellet was resuspended in membrane buffer (15 mM Tris-Cl, 0.3 mM EDTA, 2 mM $MgCl_2$, pH 7.5) and disrupted by the homogenizer Potter-Elvehjem at 1200 rpm. Next, membranes were freeze-thawed using liquid

nitrogen, pelleted by ultracentrifugation (25 min, 40000 × *g*, 4°C), carefully washed with Tris-Sucrose buffer (20 mM Tris, 250 mM Sucrose, pH = 7.4 at 4°C), and resuspended in Tris-Sucrose buffer. The membranes were homogenized using a 23G needle (10 strokes), aliquoted, snap-frozen using liquid nitrogen, and protein concentrations were determined using a bicinchoninic acid assay (Pierce™ BCA Protein Assay; Thermo Fisher Scientific). Subsequently, the membranes were stored at −80°C until use in NanoBRET assays.

Displacement of fluorescent nanobodies and CXCL12

Approximately 0.25 µg per well of membrane extracts from NanoLuc-CXCR4-expressing HEK293T cells was added to a white flat-bottom 96-well plate. Subsequently, increasing concentrations of unlabeled ligands in HBSS, supplemented with 0.1% BSA, 1 mM $MgCl_2$, and 2 mM $CaCl_2$. The plate was spun down and incubated for 30 min at RT. Next, 316 pM nanobody-ATTO565 or 10 nM CXCL12-AZ647 (Protein Foundry) was added and incubated for 1 h at RT. Next, 15 µM furimazine substrate was added, and luminescence was measured using a PHERAstar plate reader with 610 nm/LP and 460/80 nm filters until the luminescence signal stabilized.

Mini-Gα_i recruitment

To measure CXCR4-induced mini-Gα_i recruitment, HEK293T cells were transfected with 25 ng HA-CXCR4-NanoLuc and 125 ng Venus-mini-Gα_i. After 48 h incubation, cells were washed once using PBS and maintained in HBSS, supplemented with 0.1% BSA, 1 mM $MgCl_2$, and 2 mM $CaCl_2$. For antagonist mode measurements, cells were pre-treated with increasing concentrations of small molecules or nanobodies 30 min prior to stimulation with 10 nM CXCL12 for 15 min. After incubating cells for 10 min with 15 µM furimazine, bioluminescence was measured at 475-30 nm and 535-30 nm using a PHERAstar plate reader.

cAMP measurement

cAMP accumulation in Namalwa cells was measured using the Ultra cAMP kit (Lance) according to the manufacturer's instructions. Forskolin (100 µM) and saturating concentrations (10 µM) of CXCR4 ligands

were added 30 min prior to Eu-cAMP tracer addition. HTRF was measured using a PHERAstar plate reader after excitation at 337 nm and emission at 620 and 665 nm.

Flow cytometry for CXCR4 surface expression determination

For each sample, 5 x 10^5 cells were washed with ice-cold FACS buffer (0.5% BSA (PanReac AppliChem, A6588,0100) in PBS) and resuspended in ice-cold FACS buffer containing 3 µg/mL mouse anti-CXCR4 antibody 12G5 (Thermo Fisher Scientific, 35-8800) in polypropylene 5-mL tubes (Falcon). Following incubation on ice for 1 h, samples were washed three times with excess ice-cold FACS buffer to remove unbound antibody. Subsequently, samples were resuspended in ice-cold FACS buffer containing 2 µg/mL goat anti-mouse IgG (H+L) AlexaFluor™ 488 (Thermo Fisher Scientific, A-11001). After incubation and washing as described before, samples were resuspended in ice-cold FACS buffer. Subsequently, samples were analyzed utilizing an Attune Nxt Flow Cytometer (Thermo Fisher Scientific) at the AUMC Microscopy Cytometry Core Facility (MCCF), with flow rates not exceeding 500 µL/min. Sample analysis was conducted using FlowJo version 10 (BD Biosciences) to determine CXCR4 surface expression levels.

Oligomer detection using nanobody-based BRET in lymphoid cancer cell lines

1 × 10^6 lymphoid cancer cells were seeded in a white flat-bottom 96-well plate. In case of small molecule disruption, 10 µM of IT1t or AMD070 was added to the cells. Subsequently, cells were stimulated with increasing equimolar concentrations of VUN415/VUN416-NanoLuc and VUN415/VUN416-ATTO565 or ITGB1-Nb-HL555 (QvQ) in assay buffer (HBSS, supplemented with 0.1% BSA, 1 mM $MgCl_2$, and 2 mM $CaCl_2$). For oligomer detection on PBMCs derived from CLL patients, 31.6 nM of VUN416- NanoLuc/-ATTO565 detection nanobodies were added with an ATTO565: NanoLuc ratio of 0.25 ($BRET_{min}$) or 19 ($BRET_{max}$). After incubation for 2 h at RT, cells were washed twice with PBS, and assay buffer was added. Subsequently, fluorescence of fluorescently labeled nanobodies was measured using a CLARIOstar plate reader at 563/30 nm excitation and 592/30 nm emission. After the addition of 15 µM furimazine substrate, luminescence was measured using a PHERAstar plate reader with 610 nm/LP and 460/80 nm filters until the luminescence signal stabilized.

Lentivirus production and transduction

MEC-1 and RPCI-WM1 cell lines with inducible HA-CXCR4 expression and Namalwa and Z-138 cell lines with constitutive siRNA CXCR4 or scramble shRNA expression were generated by lentiviral transduction, as previously described (*6, 15*). Briefly, lentivirus was produced for 48 h after co-transfecting four dishes of 2 × 10^6 HEK293T cells with HA-CXCR4 pLenti6.3/To/V5-DEST, pLKO.1 puro CXCR4 siRNA-1/2 or plKO.1 scramble shRNA together with pRSV-REV, pMDLg/pRRE and pMD2.g packaging vectors, using PEI as transfection reagent. Lentivirus solution from four dishes was pooled, cleared by centrifugation for 10 min at 500 × g, and filter-sterilized. Subsequently, the lentivirus was ultracentrifuged for 1 h at 70000 x g, and the supernatant was discarded until approximately 1 mL of concentrated lentivirus solution was left. This lentivirus solution was then aliquoted and stored at -80 °C until lentiviral transduction. On the day of lentiviral transduction, 100 µL of concentrated lentivirus solution was added to 1 × 10^^{6} cells in 1 mL. Subsequently, cells were incubated for three days before the addition of the appropriate antibacterial selection agent. Knockdown efficiency and enhanced CXCR4 surface expression in the different cell lines were validated by determining CXCR4 surface expression levels as described before. CXCR4 expression in the doxycycline-inducible cell lines was induced using 1 µg/mL doxycycline (Sigma-Aldrich).

dSTORM microscopy

Sample preparation

RPCI-WM1, Z-138 and CHO-K1 cells were fixed using 4% paraformaldehyde (PFA) in PBS for 15 min at 37°C. Next, cells were washed once and resuspended in FACS buffer (0.05% BSA in PBS). The fixated cells were then subjected to staining with VUN415-AF647 at RT for 1 h. Unbound VUN415-AF647 was removed through a series of three consecutive washing steps using FACS buffer. 1 x 10^6 cells were added to a poly-l-lysine (Sigma)-coated coverslip (VWR) in a 6-well plate (Greiner Bio-One). The coverslip was subjected to centrifugation in the 6-well plate at 500 x g for 15 min using a plate centrifuge (Eppendorf). Following this, the samples were stored in suspension in a dark environment at 4°C until the time of readout.

Before imaging, samples were mounted in oxygen scavenger-containing Glox buffer to facilitate blinking conditions. Glox buffer was prepared as described previously (*16*). Briefly, the following stock solutions were prepared and stored at -80°C: 1M Cysteamine (MEA) in 250 mM (Sigma, in 250 mM HCl), 70 mg/mL glucose-oxidase (Sigma-Aldrich), and 4 mg/mL catalase (Sigma-Aldrich). When mounting the sample, the final buffer was prepared freshly by diluting stock solutions of MEA, glucose-oxidase plus catalase, and glucose solution in 50 mM Tris pH 8.0 (final concentrations: 100 mM MEA, 700 µg/mL glucose oxidase, 40 µg/mL catalase, 5% w/v glucose). To prevent oxygen from entering the sample during imaging, coverslips were mounted on cavity slides (Sigma-Aldrich) filled with imaging buffer. A vacuum seal was created by removing surplus buffer from the sides of the coverslip.

Imaging

Imaging was performed on a Ti-E microscope (Nikon) equipped with a 100x Apo TIRF oil immersion objective (NA 1.49) and Perfect Focus System 3 (Nikon). A Lighthub-6 laser combiner (Omicron) containing a 647 nm laser (LuxX 140 mW, Omicron) and a 405 nm diode laser (Power Technology, 15 mW), together with optics allowing for a tunable angle of incidence, was used for excitation. Illumination was adjusted for (pseudo-) total internal reflection fluorescence (TIRF) microscopy to remove out-of-focus signal. To separate emission light from excitation light, a quad-band polychroic mirror (ZT405/488/561/640rpc, Chroma) and a quad-band emission filter (ZET405/488/561/640m, Chroma) were used. Detection of the emission signal was done using a Hamamatsu Flash 4.0v2 sCMOS camera. Image stacks were acquired with a 30 ms exposure time, 50-100% laser power of the 647 laser, 3-5% laser power of the 405 laser, which was increased during imaging, and 5000 images per field of view. Components were controlled using MicroManager (*17*).

Data analysis

Acquired stacks were analyzed using v.1.2.1 of a custom ImageJ plugin called DoM (Detection of Molecules) (https://github.com/ekatrukha/DoM_Utrecht), as previously described (*16*). Briefly, each image in an acquired stack was convoluted with a two-dimensional Mexican hat kernel, which matches the microscope's point spread function (PSF) size. The resulting intensity histogram was utilized to

create a thresholded mask that was used to calculate the centroids on the original image. These centroids were used as initial values to perform unweighted nonlinear least squares fitting with a Levenberg-Marquardt algorithm to an asymmetric two-dimensional Gaussian PSF, allowing for the sub-pixel localization of particles. The acquired localization output by DoM was imported into the application ClusterViSu (https://github.com/andronovl/SharpViSu) that conducts a statistical cluster analysis based on Ripley's K-function and Voronoi segmentation, as previously described (*18*). Eight areas per sample were examined for the RPCI-WM1 and Z-138 samples, with an average area of 35 ± 10 μm^2 and 27 ± 7 $\mu m^{2,}$ respectively. Four areas per sample were examined for the CHO-K1 and non-specificity control samples (i.e., displacement with an excess of CXCR4 antagonist AMD3100). Selected areas did not overlap or come in contact with the edges of the corresponding analyzed cell. Ripley's K-function was calculated, and Voronoi segmentation was conducted for the indicated areas, and localization distributions were compared to a random distribution based on a similar surface area and number of localized points by conducting Monte-Carlo simulations. Segmentation was conducted subsequently by automatic thresholding of the cluster map. Quantitative output, including cluster area, diameter and stoichiometry, was determined.

Spatial intensity distribution analysis (SpIDA)

For SpIDA analysis, 2.5×10^5 HEK293AD cells were grown on glass coverslips in six-well plates. The next day, cells were transfected with 600 ng of CXCR4-EYFP using Effectene transfection reagent (Qiagen) according to the manufacturer's protocol. The next day, the coverslip was loaded into the Attofluor imaging chamber (Thermo Fisher Scientific). Prior to imaging, cells were stimulated for 30 min with 10 µM IT1t, AMD0070, or TG-0054 in HBSS supplemented with 0.1% BSA. Imaging was performed using a commercial laser-scanning confocal microscope (Leica SP8) equipped with a 63×/1.40 NA oil immersion objective, a white light laser (WLL), and photon counting hybrid detectors. For excitation, 514 nm lines of the WLL were used, and for the detection of EYFP, emission bands of 520 nm to 600 nm were used. Images were acquired using 15% laser power. The image format was xy, and the image size was set to 512 × 512 pixels with a 50-nm pixel size. For image analysis, the open-source custom-made code (https://github.com/PaoloAnnibale/MolecularBrightness) was loaded onto the Igor Pro software

(WaveMetrics). Polygonal region of interest (ROI) selection was performed to avoid regions with non-homogeneous fluorescence distribution (e.g., membrane raffles, clusters).

Phosphoproteomics

Sample preparation

Cell pellets were lysed in 8 M urea with 50 mM ammonium bicarbonate (pH 8, Sigma-Aldrich) with 1× Protease inhibitor cocktail EDTA (Roche) and 1× PhosSTOP (Roche). Sonication was performed with a Bioruptor (Diagenode) sonicator for 5 cycles (30 s on, 30 s off) at 4 °C. The lysate was spun down for 1 h at 14,000 rpm at 16 °C to pellet cell debris and DNA. Protein concentration was determined by a microplate Bradford assay (Sigma-Aldrich). For each sample, 1 mg was taken for further digestion and phosphopeptide enrichment.

Protein samples were reduced in 10 mM dithiothreitol (DTT, Sigma-Aldrich) at 20 °C for 60 min, and alkylated in the dark with 20 mM iodoacetamide (IAA, Sigma-Aldrich) at 20 °C for 30 min. An additional final concentration of 10 mM DTT was added to quench the excess IAA. 50 mM ammonium bicarbonate was used to dilute to reach a final concentration of 2 M Urea. The alkylated proteins were sequentially digested using Lys-C (Wako) and trypsin (Sigma-Aldrich) at a 1:75 enzyme-to-protein ratio, and carried out at 37 °C. The Lys-C digestion lasted for 4 h. Then, 50 mM ammonium bicarbonate was used to dilute the samples to a final concentration of 2 M urea, and digestion with trypsin was performed overnight. 3% formic acid was used to quench the digestion, and digested peptides were desalted by Sep-Pak C18 1 cc Vac cartridges (Waters), dried using a vacuum centrifuge, and stored at -80 °C for further use.

Automated Fe^{3+}-IMAC phosphopeptide enrichment

Phosphopeptides were enriched by using Fe(III)-NTA 5 µIL (Agilent Technologies) in an automated AssayMAP Bravo Platform (Agilent Technologies). Fe(III)-NTA (nitrilotriacetic acid) cartridges were first primed with 250 µL of priming buffer (99% acetonitrile (ACN), 0.1% TFA) at a flow rate of 100 µL/min and equilibrated with 250 µL of loading buffer (80% ACN, 0.1% TFA) at a flow rate of 50 µL/min. Dried peptides were dissolved in 210 µL of loading buffer and centrifuged at 14000 rpm for 10 min. Samples

were then loaded at a flow rate of 3 µL/min onto the cartridge, the flowthrough was collected into a separate plate. Cartridges were washed with 250 µL of loading buffer at a flow rate of 20 µL/min, and the phosphopeptides were eluted with 50 µL of 10% ammonia at a flow rate of 5 µL/min directly into 50 µL of 10% formic acid. Flowthroughs and elutions were dried and injected directly into a liquid chromatography-coupled mass spectrometer.

LC–MS/MS analyses

The phosphoproteome measurement was performed on an Orbitrap Exploris 480 mass spectrometer (Thermo Fisher Scientific) coupled with an UltiMate 3000 UHPLC system (Thermo Fisher Scientific) fitted with a µ-precolumn (C18 PepMap100, 5 µm, 100 Å, 5 mm × 300 µm; Thermo Fisher Scientific). Samples were analyzed in triplicate and separated on an analytical column (Poroshell 120 EC-C18, 2.7 µm, 50 cm × 75 µm, Agilent Technologies) with a 115-min gradient. Peptides were first eluted at a constant flow rate of 300 nl/min using 9 to 36% solvent B (0.1% v/v formic acid in 80% acetonitrile) over 97 min, raised to 99% in 3 min, then held for 3 min and equilibrated in 9% B for 1 min. The mass spectrometer was operated in data-dependent mode. Electrospray ionization was performed at a 2.1 kV static spray voltage; the temperature of the ion transfer tube was set to 275 °C, and the RF lens voltage was set to 55%. Full scan MS spectra from the m/z range of 375-1600 were acquired at a resolution of 60,000 after accumulating to the ‘Standard’ pre-set automated gain control (AGC) target. Higher energy collision dissociation (HCD) was performed with 35% normalized collision energy (NCE), at an orbitrap resolution of 30,000. Dynamic exclusion time was set to 90 s, and a 0.7 m/z isolation window was used for fragmentation.

Database Search and Analysis

Data search was performed using MaxQuant (version 2.1.3.0) with an integrated Andromeda search engine, against the human Swiss-Prot protein database (Downloaded on October 10th, 2022, containing 20,398 reviewed sequences). Digestion was defined as Trypsin/P, and a maximum of 2 missed cleavages was allowed. Cysteine carbamidomethylation was set as a fixed modification. Protein N-terminal acetylation, methionine oxidation, and phosphorylation on serine, threonine, and tyrosine were

set as variable modifications. Label-free quantification (LFQ) and the match-between-runs feature were enabled for protein quantification. A false discovery rate (FDR) of 1% was applied to both peptide spectrum matches (PSMs) and protein identification using a target-decoy approach. For total proteome measurements, intensity-based absolute quantification (iBAQ) was enabled.

Quantitative data filtering was conducted using the Perseus software (version 1.6.14.0). Proteins cross-matched to bovine contaminants were removed along with potential contaminants, reverse peptides, and proteins only identified by sites. LFQ intensities were log2-transformed. Proteins that were quantifiable in at least two out of three replicates were retained. Imputation was performed based on the normal distribution.

Constitutive cell migration assessment

To assess the potential effect of CXCR4 cluster disruption on basal cell motility, Z-138 cells with a viability of > 90% were prepared at a concentration of 6×10^6 cells/mL in standard growth (FBS-supplemented) media. These cells were treated with 1 µM of either IT1t, AMD3100, VUN401, VUN415 or vehicle. After an incubation period of 1 hour at 37°C, the cells were mixed 2:1 with ice cold BD Matrigel™. All plastics, including tips, eppindorf tubes and imaging slides were pre-chilled before use. Subsequently, 6 µL of the cell suspension was loaded into the central imaging chamber of an Ibidi µ-slide Chemotaxis (IbiTreat surface modification), according to manufacturer's instruction. The Matrigel was allowed to solidify at 37°C for 30 minutes before filling the reservoirs flanking each chamber with media containing equal concentration of the compound.

Time-lapse video microscopy was conducted by capturing an image with a 10x phase contrast objective, every 5 minutes for 4 hours, using a Nikon Ti2 microscope equipped with temperature (37°C) and CO_2 (5%) control. Image analysis was performed using the open-source image processing software ImageJ2, version 2.14.0/1.54f. The manual tracking plugin was employed to analyze the trajectories of cells exhibiting high basal motility. For each condition, 5 different cells were included in the conducted analysis. The Ibidi Chemotaxis and Migration Tool ImageJ plugin was utilized to generate Rose plots and extract average trajectory information.

Resazurin assays for venetoclax sensitization

A total of 3 × 10^4 Z-138, Jeko-1 and Maver-1 cells with a viability of > 90% were seeded in serum-free IMDM in a black 96-well plate (Greiner Bio-One). For primary cultures, 3 × 10^4 PBMCs of CLL patients were thawed and seeded in IMDM supplemented with 10% FBS in a black 96-well plate. After 1 h, cells were treated with increasing concentrations of venetoclax in the absence or presence of 10 μM IT1t, AMD070, AMD3100, TG-0054, or VUN401. After 48 h incubation, 44 μM resazurin was added to the culture medium. After 1 h incubation, fluorescence cytotoxicity read-out was performed using a CLARIOstar plate reader at 540/30 nm excitation and 590/30 nm emission.

FACS viability assays for venetoclax sensitization

A total of 3 × 10^4 Z-138, Jeko-1, and Maver-1 cells with a viability of > 90% were seeded in serum-free IMDM in a transparent flat 96-well plate (Greiner Bio-One). After 1 h, cells were treated with increasing concentrations of venetoclax in the absence or presence of 10 μM IT1t, AMD070, AMD3100, TG-0054, or VUN401 and 20 μM pan-caspase inhibitor qVD-OPH. After 48 h incubation, 100 nM MitoTracker Orange (ThermoFisher Scientific, M7510) and 20 nM Topro-3 (ThermoFisher Scientific, T3605) were added according to the manufacturer's guidelines. Well contents were transferred to polypropylene 5 mL tubes (Falcon) and analyzed using an Attune NxT Flow Cytometer.

Synergy assessment was done using the Bliss independence model, where ΔBliss scores for two compounds were calculated according to the following formulas:

(1) $\Delta Bliss = E_{Expected} - E_{Observed}$

(2) $E_{Expected} = 100\left(\frac{E_A}{100}\right)\left(\frac{E_B}{100}\right)$

The Bliss independence model was used to assess whether the combined effect of compounds A and B is higher than the expected effect ($E_{Expected}$) based on the relative individual effects (E_A and E_B).

Spheroid assays

PBMCs of CLL patients were thawed, plated in ultra-low attachment plates, and centrifuged for 10 min at 1000 rpm and subsequently incubated for 24 h to allow spheroid formation. Three-dimensional (3D) cultures were cultured in IMDM supplemented with 10% FBS and 1% P/S and were stimulated and

treated as indicated. Culture plates were placed in an IncuCyte live-cell imager (Essen Biosciences) in an incubator at 37ºC and 5% CO_2. Scans were taken every 5 h using the single spheroid assay for live-cell analysis application and 4x magnification. Spheroid area was quantified using IncuCyte software as a proxy for spheroid growth. Corresponding step-by-step protocols were previously described (*19*).

After culture, spheroids were resuspended and disintegrated to ensure proper antibody staining. Cells were incubated with monoclonal antibodies for surface staining for 30 min at 4ºC. Cells were stained with antibodies against CD4 (AF700-labeled OK-T4, 56-0048-82, eBioscience), CD8 (PE-Cy7-labeled RPA-T8, 25-0088-42, eBioscience), CD19 (APC-labeled HIB19, 555415, BD Biosciences) and CD5 (PerCP-eF710-labeled UCHT2, 46-0059-42, eBioscience) for gaiting and with anti- CD25 (PE-conjugated clone M-A251, 555432, BD Biosciences) and Fixable Viability Dye eFluor™ 780 (ThermoFisher, 65-0865-14) to measure T cell activation and viability. Samples were measured on a Canto II flow cytometer (BD Biosciences). Samples were analyzed using FlowJo software.

Data analysis

All graphs and bar plots were visualized, and statistical analyses were performed using Prism version 10.0 (GraphPad) unless indicated otherwise. Curves were fitted using least squares nonlinear regressions, assuming a sigmoidal fit (for concentration-response curves). The significance of differences was determined as indicated in the figure legends. Schematics for assay formats were generated using Biorender.com.

Data Availability

The phosphoproteomics data have been deposited into the ProteomeXchange Consortium through the PRIDE partner repository with the dataset identifier PXD053673.

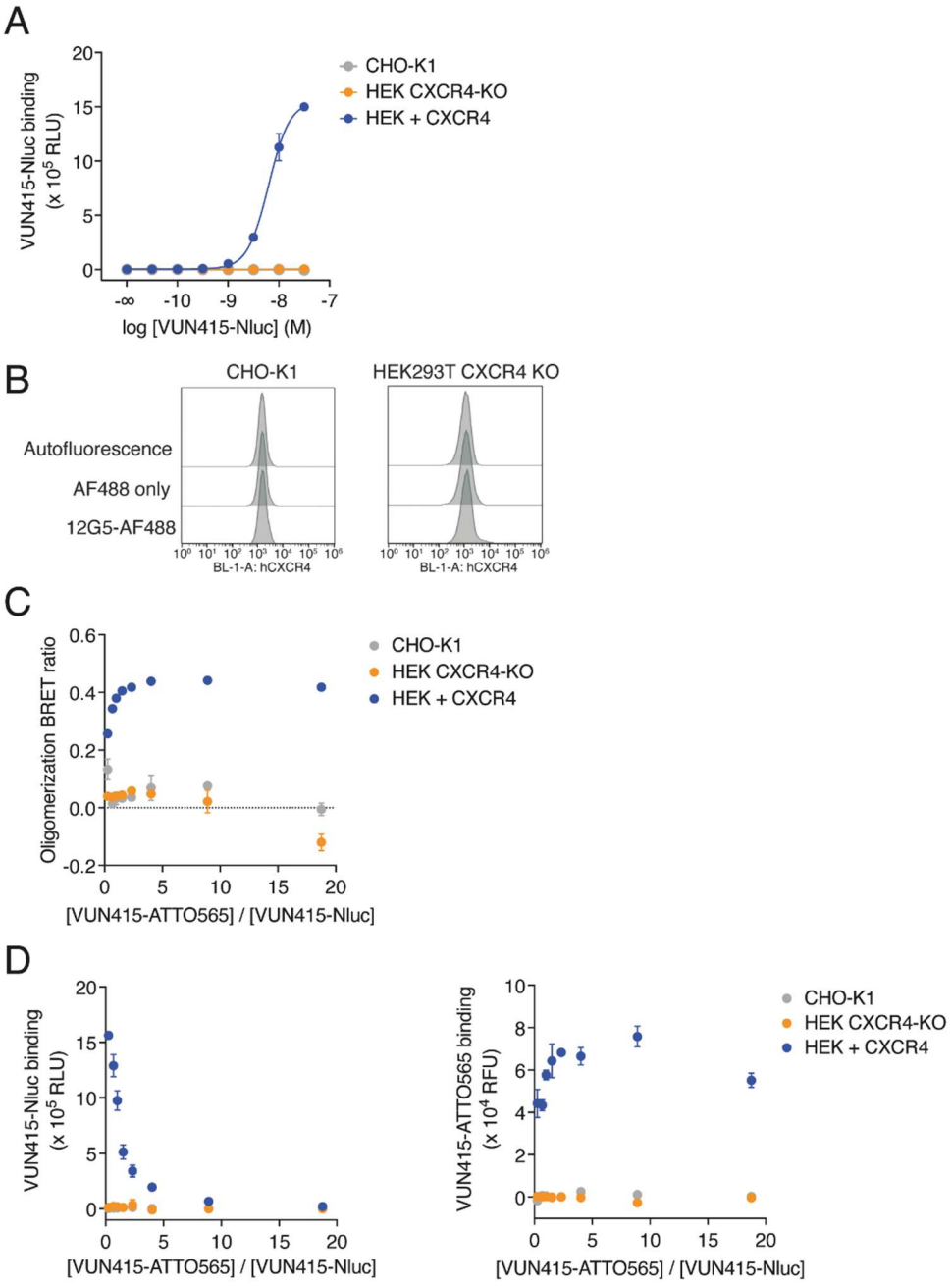

Figure S1. Controls for nanobody-based BRET to detect oligomers of transfected CXCR4. A VUN415-NanoLuc binding curves in CHO-K1 (grey symbols and line obscured by CXCR4 KO), HEK293T CXCR4 CRISPR Cas9 KO and CXCR4-overexpressing HEK293T cells. **B** CXCR4 surface expression levels in CHO-K1 and HEK293T CXCR4 KO cell lines detected by flow cytometry with CXCR4 antibody 12G5. In the same experiment, autofluorescence was determined and cells were treated with secondary antibodies alone as control conditions. **C** Nanobody-based saturation setup measurement of CXCR4 oligomerization in CHO-K1, HEK293T CXCR4 CRISPR Cas9 KO and CXCR4-overexpressing HEK293T cells. 31.6 nM detection nanobodies with increasing ratios of VUN415-ATTO565 to VUN415-NanoLuc were used for oligomer detection. **D** Binding curves of VUN415-NanoLuc and VUN415-ATTO565 in parallel of oligomerization detection experiment in CHO-K1, HEK293T CXCR4 CRISPR Cas9 KO and CXCR4-overexpressing HEK293T cells. Data are mean ± SD and are representative of three independent experiments, each performed in triplicate **(A, C, D)** or are representative histograms of three independent experiments **(B)**.

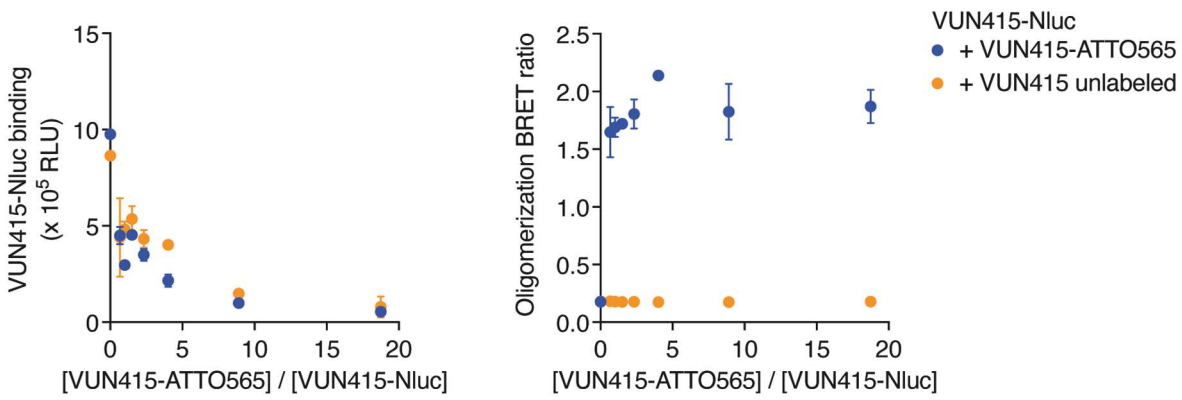

Figure S2. No oligomerization BRET signal when using VUN415-NanoLuc with unlabeled VUN415 instead of VUN415-ATTO565. VUN415-NanoLuc binding and nanobody-based saturation setup measurement of CXCR4 oligomerization in CXCR4-overexpressing HEK293T cells. 31.6 nM nanobodies with increasing ratios of VUN415(-ATTO565) to VUN415-NanoLuc were used for oligomer detection. Data are mean ± SD and are representative of three independent experiments, each performed in triplicate.

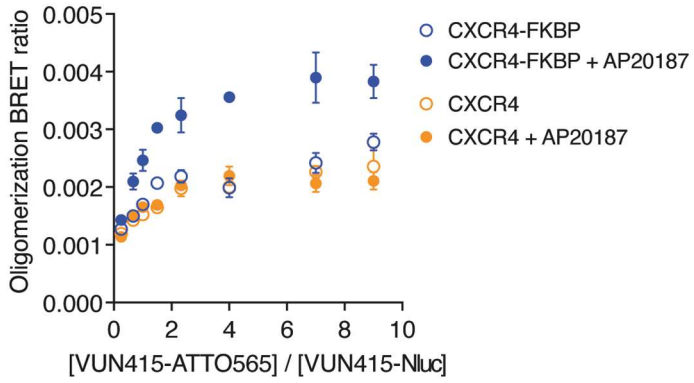

Figure S3. The FKBP domain demonstrates the specificity of the nanobody-based method to detect forced dimerization at low expression levels. Nanobody-based saturation setup measurement of CXCR4 oligomerization in CXCR4 and CXCR4-FKBP overexpressing HEK293T cells. Cells were stimulated with AP201827 (1 uM) to induce receptor dimerization of CXCR4-FKBP. 31.6 nM detection nanobodies with increasing ratios of VUN415-ATTO565 to VUN415-NanoLuc were used for oligomer detection. Data are mean ± SD and are representative of three independent experiments, each performed in triplicate.

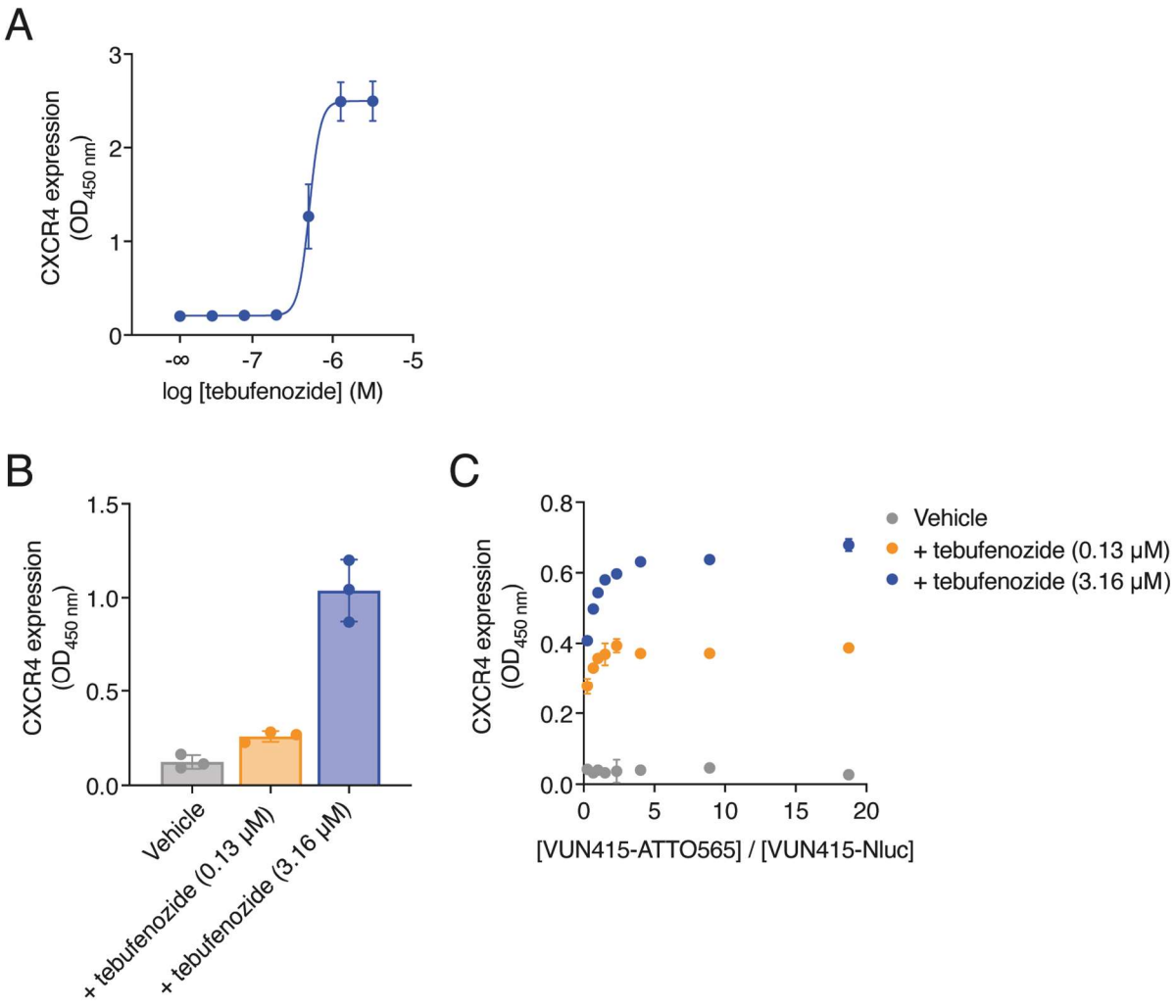

Figure S4. Nanobody-based BRET method validates expression dependency for oligomerization of transfected CXCR4. A, B ELISA-based measurement of receptor expression levels for ecdysone-inducible CXCR4 in HEK293T cells using equimolar **(A)** and saturation setup **(B)**. Stimulation with increasing concentrations of tebufenozide to induce receptor expression. **C** Nanobody-based saturation setup measurement of ecdysone-inducible CXCR4 oligomerization in HEK293T cells. 31.6 nM detection nanobodies with increasing ratios of VUN415-ATTO565 to VUN415-NanoLuc were used for oligomer detection. Data are mean ± SD and are representative of three independent experiments, each performed in triplicate.

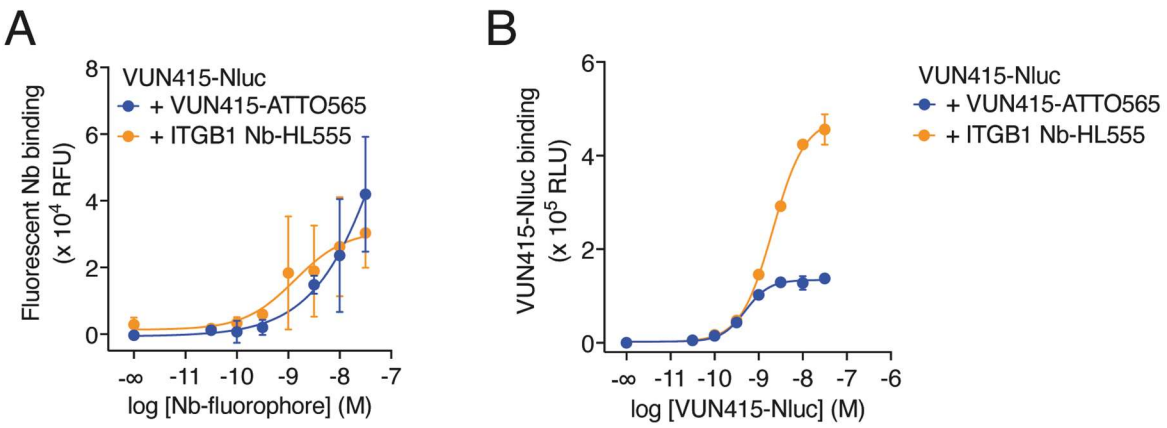

Figure S5. **Absence of oligomerization BRET signal is not due to a lack of ITGB1-Nb-HL555 binding. A, B** Binding curves of increasing concentrations of VUN415-ATTO565 and ITGB1-Nb-HL555 **(A)** or VUN415-NanoLuc **(B)** in parallel with the oligomerization detection experiment in Namalwa cells. Data are mean ± SD and are representative of three independent experiments, each performed in triplicate.

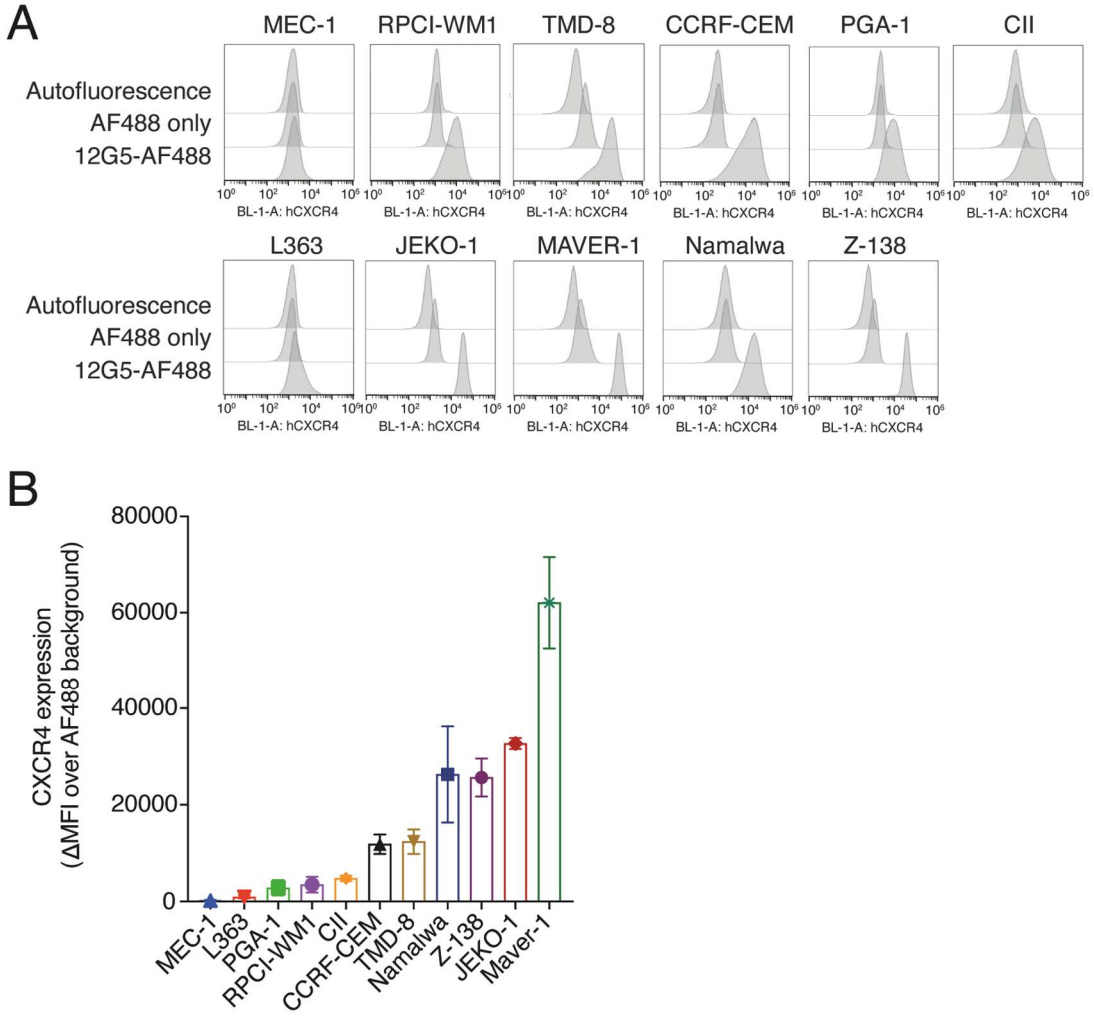

Figure S6. CXCR4 expression levels for the complete panel of lymphoid cancer cell lines. Histograms (A) and mean fluorescence intensity values (B) of CXCR4 surface expression levels in the panel of lymphoid cancer cell lines detected by flow cytometry with CXCR4 antibody 12G5. In the same experiment, autofluorescence was determined, and cells were treated with secondary antibodies alone as control conditions. Expression profiles, corrected for AF488 background, are displayed as mean ± SEM of the panel of lymphoid cancer cell lines. Data are representative histograms of three independent experiments.

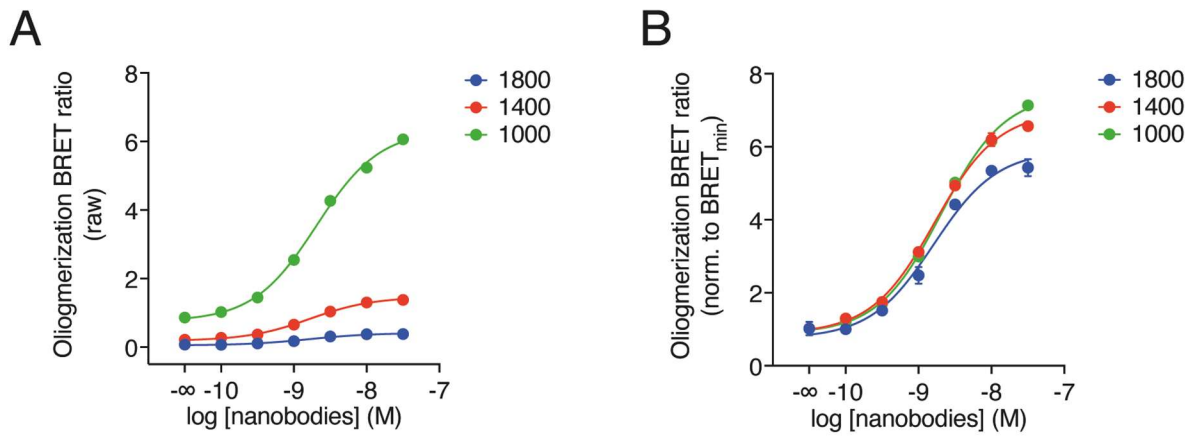

Figure S7. Plate reader gain settings do not influence normalized oligomerization BRET$_{max}$ values. Nanobody-based equimolar setup measurement of CXCR4 oligomerization in Z-138 cells. Increasing equimolar concentrations of detection nanobodies VUN415-NanoLuc and VUN415-ATTO565 were used. Curves of raw **(A)** and BRET$_{min}$-normalized (**B)** BRET ratios for different gain settings are shown. Data are mean ± SD and are representative of three independent experiments, each performed in triplicate.

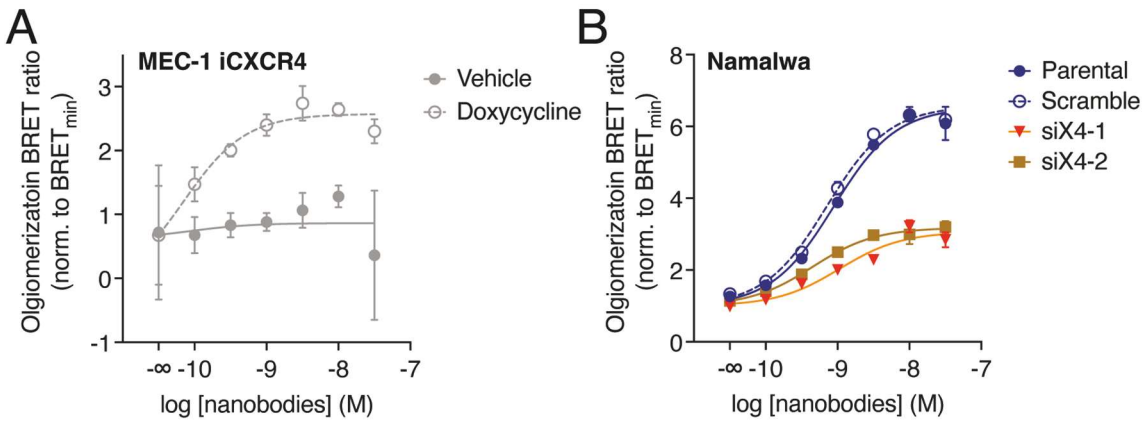

Figure S8. Validation of knockdown and upregulation in genetic approaches to modulate CXCR4 oligomerization. **A, B** CXCR4 surface expression levels and nanobody-based BRET measurement of oligomeric complexity in doxycycline-stimulated MEC-1 iCXCR4 cells **(A)** or Namalwa ± scramble shRNA or CXCR4 siRNA-1/2 cells **(B)**. Increasing equimolar concentrations of VUN415-NanoLuc and VUN415-ATTO565 were used for oligomer detection. Data are the mean ± SD and are representative of three independent experiments, each performed in triplicate.

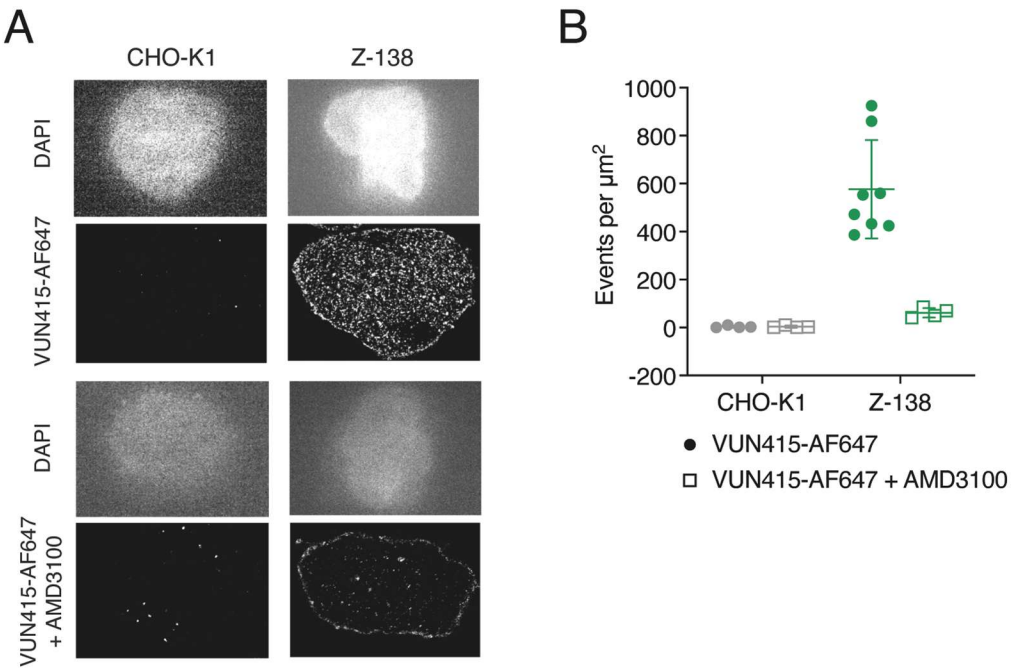

Figure S9. Additional dSTORM data. A Reconstructed dSTORM images of VUN415-Alexa647 stains in the presence or absence of excess AMD3100 and corresponding DAPI stains of CHO-K1 and Z-138 cells. **B** CXCR4 density assessment on CHO-K1 and Z-138 cells. Pooled mean fractions ± SEM are of four or eight analyzed areas, from two independent experiments per cell line.

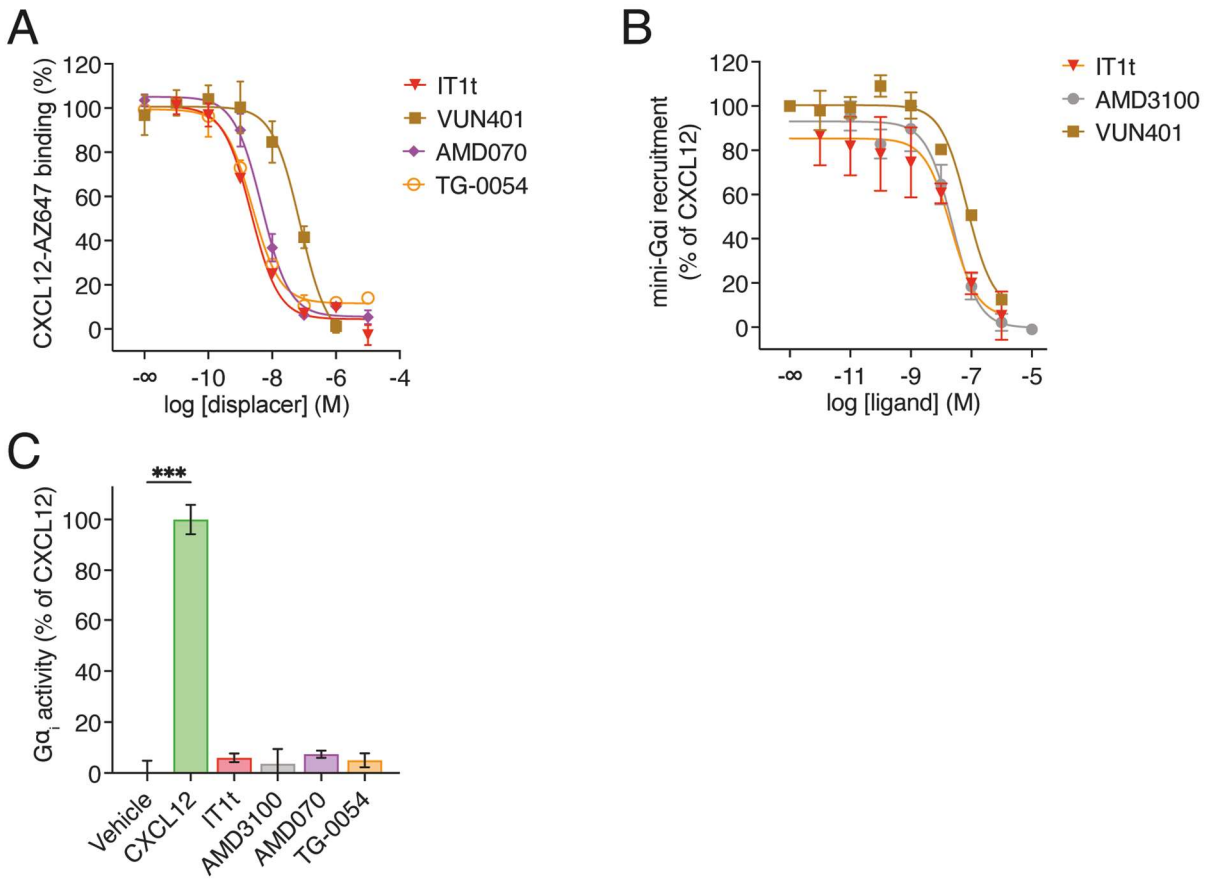

Figure S10. Characterization of receptor binding and signaling activity for the panel of CXCR4 antagonists. A BRET-based measurement of 10 nM CXCL12-AZ647 binding to NanoLuc-CXCR4 (Nluc-CXCR4) in HEK293T cells after pre-treatment with increasing concentrations of unlabeled ligands, as indicated. Values are BRET signals normalized to 'no fluorescent ligand' (0%) and 'fluorescent ligand only' (100%) conditions and represent mean ± SEM from three independent experiments performed in duplicate. Data, normalized to the buffer-only condition, are the mean ± SD and are representative of three independent experiments, each performed in triplicate. **B** BRET-based measurement of CXCL12-induced recruitment of mini-$G\alpha_i$ to CXCR4, after pre-treatment with increasing concentrations of unlabeled ligands, as indicated. Values are BRET signals normalized to buffer (0%) and 'CXCL12 only' (100%) conditions and represent mean ± SEM from three independent experiments performed in duplicate. **C** HTRF-based measurement of cAMP levels in Namalwa cells stimulated with 100 µM of FSK and saturating concentrations (10 µM) of indicated CXCR4 ligands. Values represent mean ± SEM from three experiments performed in triplicate. *** P <0.001, according to one-way ANOVA followed by Dunnett's post hoc test.

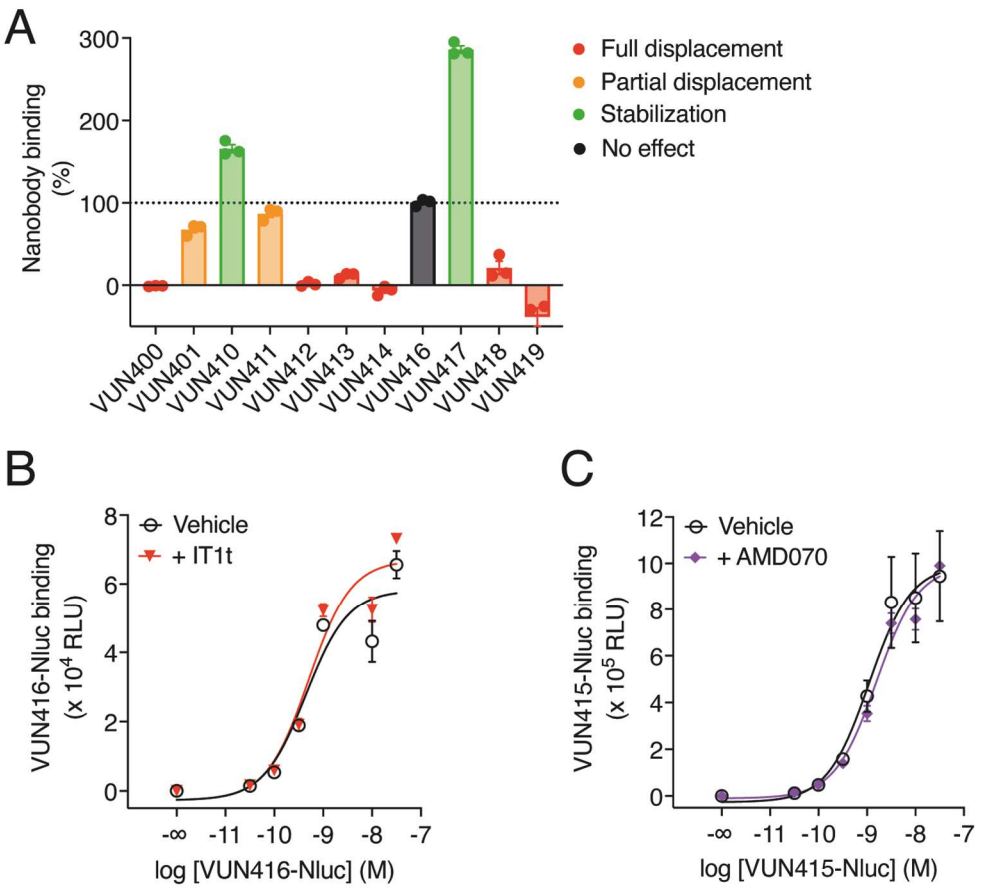

Figure S11. Screen identifies VUN416 as non-IT1t-competitive nanobody and VUN415 as non-AMD070 competitive nanobody. A BRET-based measurement of indicated nanobody-ATTO565 (1 nM) binding in presence of IT1t (10 μM) using membrane extracts from NanoLuc-CXCR4-expressing HEK293T cells. Dotted line indicates the fluorescent ligand only condition. Data, normalized to the fluorescent ligand only condition, are the pooled mean ± SEM of three independent experiments, each performed in duplicate. **B** Binding curves of increasing concentrations VUN416-NanoLuc in the absence or presence IT1t (10 μM), in parallel with the oligomerization detection experiments in Z-138 cells. Data are mean ± SD and are representative of three independent experiments, each performed in triplicate. **C** Binding of increasing concentrations of VUN415-NanoLuc in the absence or presence of AMD070 (10 μM), in parallel of the oligomerization detection experiment in Z-138 cells. Data, normalized to the buffer-only condition, are the mean ± SD and are representative of three independent experiments, each performed in triplicate.

A

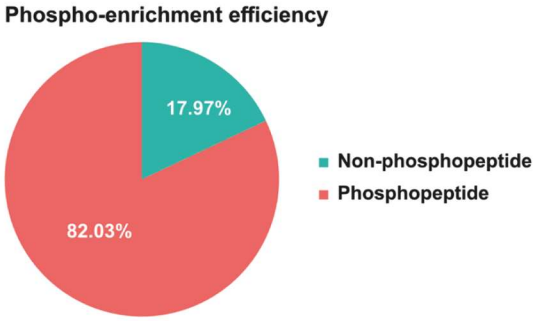

	Phosphopeptide	Non-phosphopeptide	Total
Phosphopeptide number	15,563	3,410	18,973

B

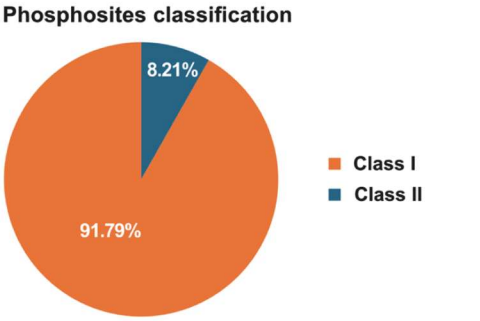

	Class I	Class II	Class III
Localization probability	x>0.75	0.25≤x≤0.75	x<0.25
Phosphopeptide number	15,199	1,360	0

C

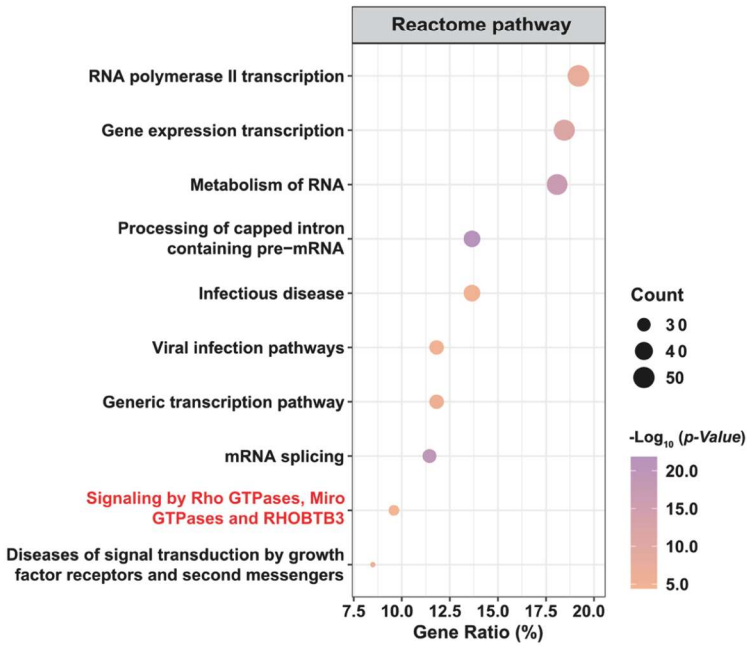

Figure S12. Quality control of phosphoproteomics samples. A and B Evaluation of phospho-enrichment efficiency (A) and phospho-site classification (B). **C** Biological pathways modulated by CXCR4 cluster disruption by IT1t. Evaluation of the pathways modulated by cluster disruptors IT1t following stimulation for 60 minutes, displayed as a Gene Ontology plot.

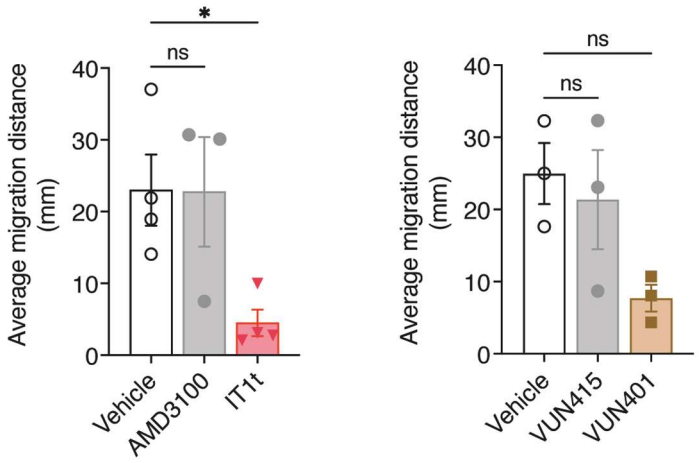

Figure S13. CXCR4 monomerizing ligands impair the basal migration of an MCL cell line. The average traveled distance of MCL Z-138 cells after four hours following treatment with 1 μM of AMD3100, IT1t, VUN415, or VUN401. Data are the pooled mean ± SEM of at least three independent experiments. * $P < 0.05$ compared to vehicle, according to one-way ANOVA followed by Dunnett's post hoc test.

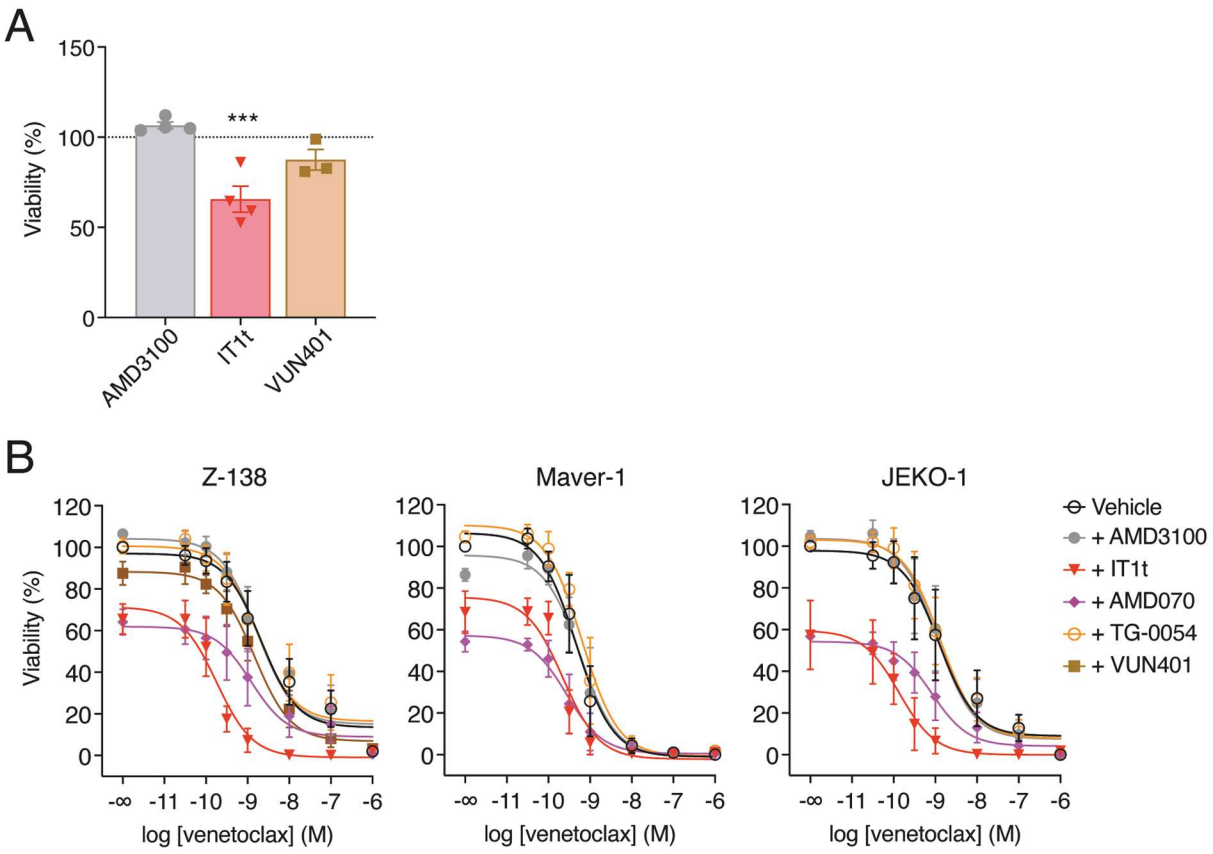

Figure S14. CXCR4 monomerizing ligands inhibit the viability of Z-138, Maver-1, and JEKO-1 cells. **A** FACS-based measurement of cell death in MCL Z-138 cells after 48 h treatment in the absence (vehicle) or presence of indicated ligands (10 μM). Data are the pooled mean ± SEM of at least three independent experiments. *** $P < 0.001$, compared to 'vehicle' condition (100%), according to one-way ANOVA followed by Dunnett's post hoc test**. B** FACS-based measurement of cell death in indicated lymphoid cancer cell lines after 48 h treatment with venetoclax in the absence (vehicle) or presence of indicated ligands (10 μM). Data, normalized to the 'no venetoclax' condition, are the pooled mean ± SEM of at least three independent experiments, each performed in triplicate.

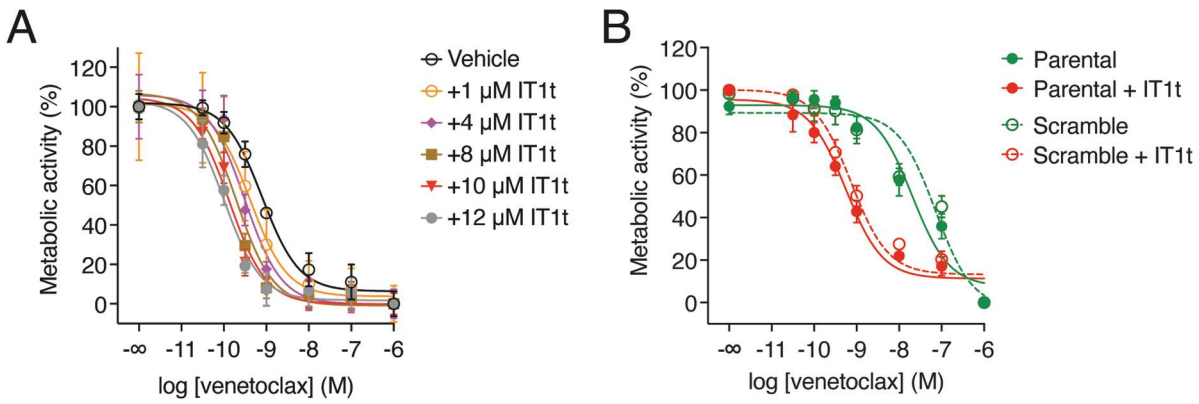

Figure S15. Sensitization of MCL cell line Z-138 to venetoclax depends on IT1t dose and high CXCR4 expression. A Resazurin-based measurement of metabolic activity in Z-138 cells after 48 h treatment with increasing concentrations of venetoclax in the absence (vehicle) or presence of five increasing concentrations of IT1t. Data, normalized to the 'no venetoclax, vehicle' condition, are the pooled mean ± SEM of at least three independent experiments, each performed in triplicate. **B** Resazurin-based measurement of metabolic activity in Z-138 upon CXCR4 knock down (right) or negative controls (left) and 48 h treatment with a concentration range of venetoclax in the absence (vehicle) or presence of IT1t (10 µM). Data, normalized to the 'no venetoclax' condition, are the pooled mean ± SEM of at least three independent experiments, each performed in triplicate. * $P < 0.05$, ** $P < 0.01$, compared to vehicle, according to unpaired t-test.

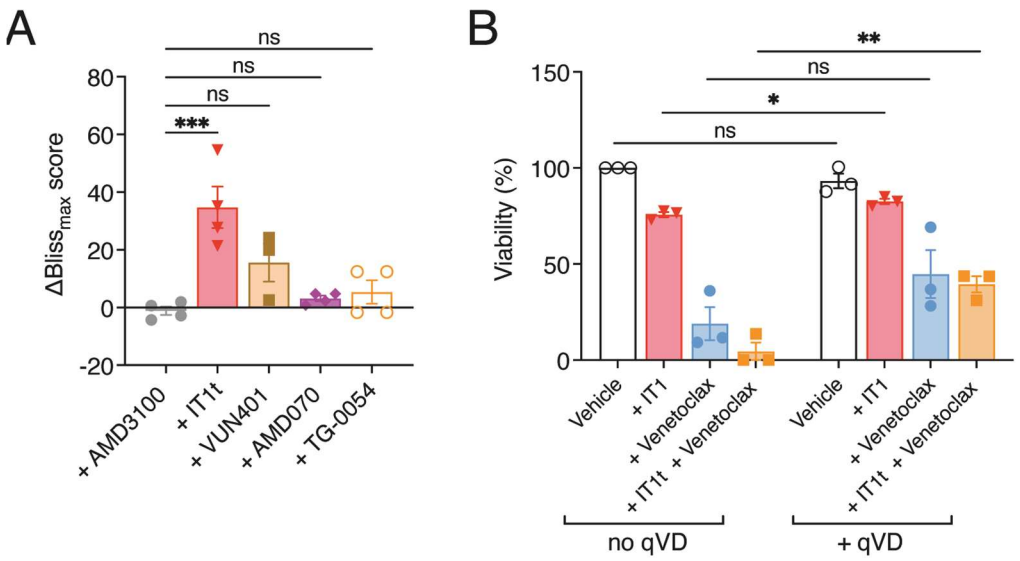

Figure S16. CXCR4-monomerizing ligands sensitize multiple MCL cell lines to venetoclax-induced apoptosis in a synergistic manner. A ΔBliss score assessment on the FACS-based cell death measurements in Z-138 after 48 h treatment with venetoclax in the absence (vehicle) or presence of indicated ligands (10 μM). Maximal ΔBliss scores (ΔBliss$_{max}$) at variable venetoclax concentrations are displayed (100 nM venetoclax for VUN401, 1 nM venetoclax for AMD070 and AMD3100, 316 pM venetoclax for IT1t, and 100 pM venetoclax for TG-0054). Data are the pooled mean ± SEM of at least three independent experiments. *** $P < 0.001$, compared to vehicle, according to one-way ANOVAs followed by Dunnett's post hoc test. **B** FACS-based measurement of cell death in Z-138 after 48 h treatment with venetoclax (3 nM), IT1t (10 μM), or combined in the absence or presence of the pan-caspase inhibitor qVD-OPH (20 μM). Data are the pooled mean ± SEM of at least three independent experiments. * $P < 0.05$, ** $P < 0.01$, compared to 'no qVD' condition, according to unpaired t-tests.

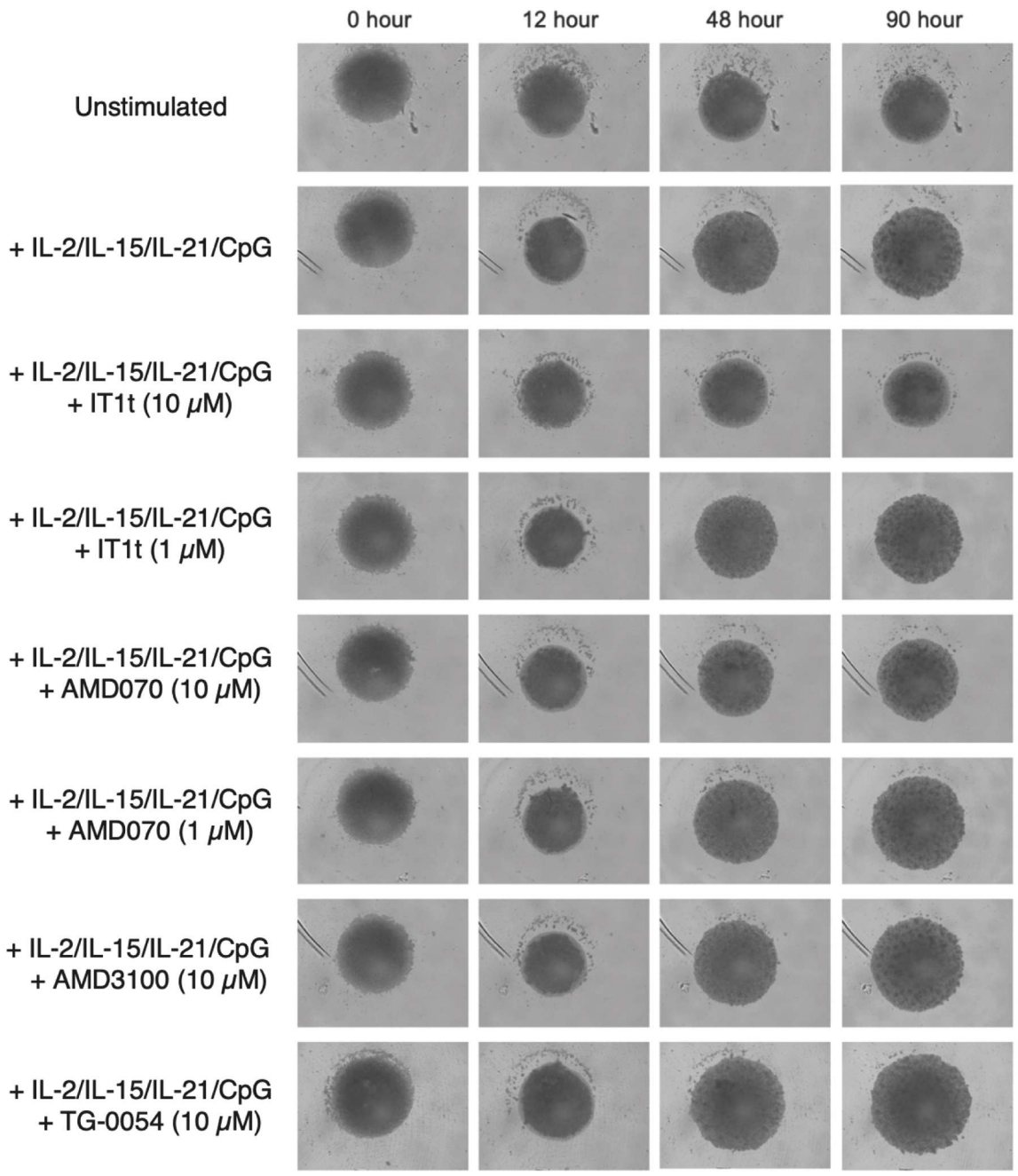

Figure S17. CXCR4-monomerizing ligands selectively inhibit growth in a CLL patient-derived spheroid model. Effects of indicated CXCR4 antagonists on IL-2/IL-15/IL-21/CpG cocktail-induced growth curve in CLL patient-derived spheroid model (*19*). Representative images of a culture derived from a single patient are shown.

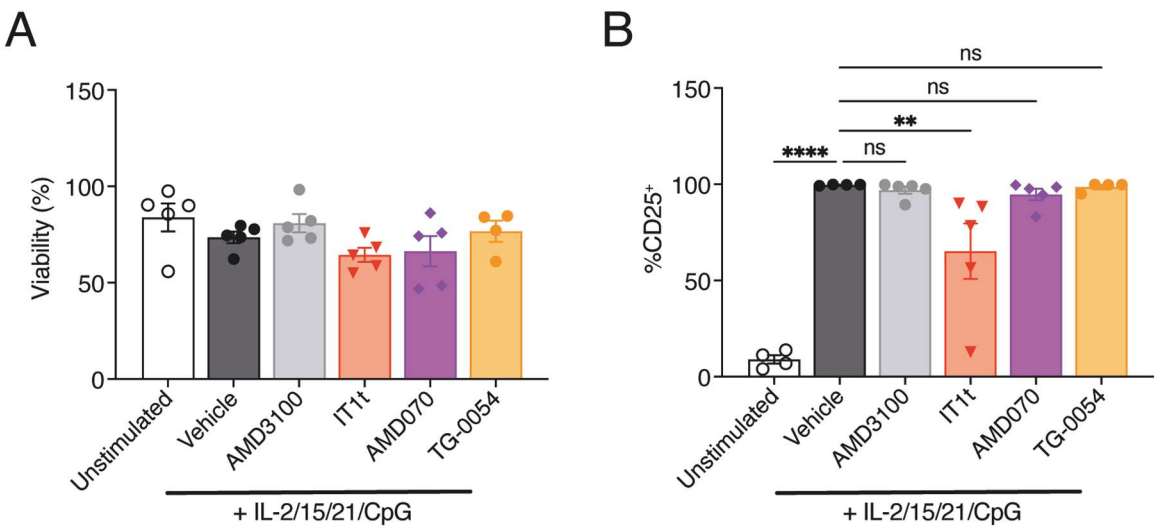

Figure S18. Spheroid growth inhibition is not due to the toxicity of compounds. A, B Effects of indicated CXCR4 antagonists (10 μM) on cell viability (**A)** and expression of activation marker CD25 **(B)** in primary CLL spheroid model after 90 hours of treatment. Data are mean ± SEM of cultures from four (TG-0054) or five individual patients. No significant difference compared to vehicle, according to one-way ANOVAs followed by Dunnett's post hoc test **(A)**. ** P < 0.01, **** P < 0.0001, compared to vehicle, according to one-way ANOVAs followed by Dunnett's post hoc test **(B)**.

Table S1. Screen for CXCR4-targeting oligomer detection nanobody with high receptor binding affinity and neutral properties. Data, normalized to the fluorescent ligand only (for CXCL12-AF647 displacement) or the vehicle condition (for modulation of CXCR4 oligomerization and inhibition of constitutive $G\alpha_{i/o}$ activation), are the pooled mean ± SEM of three independent experiments, each performed in duplicate. Significant differences ($P < 0.05$) compared to vehicle condition are indicated in bold, according to a one-sample t-test.

	CXCL12-AZ647 displacement		**Modulation CXCR4 oligomerization**		**Inhibition constitutive $G\alpha_{i/o}$ activation**	
Nb	Displacement, mean % ± SEM)	pIC_{50} mean ± SEM)	E_{max} mean ± SEM)	P	E_{max} mean ± SEM)	P
VUN400	99 ± 5	8.1 ± 0.11	1.01 ± 0.016	0.652	**0.90 ± 0.012**	**0.014**
VUN401	106 ± 9	7.1 ± 0.16	**0.87 ± 0.011**	**0.008**	1.04 ± 0.013	0.088
VUN410	92 ± 3	8.0 ± 0.08	0.99 ± 0.013	0.514	1.00 ± 0.009	>0.999
VUN411	100 ± 4	8.1 ± 0.09	**0.94 ± 0.003**	**0.002**	0.99 ± 0.004	0.163
VUN412	101 ± 3	8.3 ± 0.09	1.00 ± 0.015	0.999	0.98 ± 0.011	0.225
VUN413	103 ± 7	7.8 ± 0.16	1.02 ± 0.018	0.380	**0.93 ± 0.009**	**0.15**
VUN414	100 ± 5	8.0 ± 0.13	0.98 ± 0.007	0.117	**0.93 ± 0.001**	**0.0003**
VUN415	102 ± 5	8.7 ± 0.13	0.99 ± 0.004	0.163	1.01 ± 0.003	0.074
VUN416	105 ± 5	8.8 ± 0.12	0.98 ± 0.007	0.117	**0.97 ± 0.002**	**0.042**
VUN417	107 ± 6	7.5 ± 0.13	1.02 ± 0.010	0.194	0.99 ± 0.004	0.102
VUN418	108 ± 6	7.4 ± 0.13	**0.90 ± 0.008**	**0.002**	1.04 ± 0.010	0.165
VUN419	112 ± 6	8.4 ± 0.17	**0.90 ± 0.019**	**0.012**	1.01 ± 0.016	0.559

Table S2. Effects of CXCR4 ligands on venetoclax potency in different MCL and CLL cell lines in a resazurin readout. Data are the pooled mean ± SEM of at least three independent experiments, each performed in triplicate. Significant differences (P < 0.05) compared to vehicle condition are indicated in bold, according to a one-way ANOVA followed by Dunnett's post hoc test. * P < 0.05, ** P < 0.01, **** P < 0.0001.

	Z-138		**Maver-1**		**Jeko-1**		**PGA-1**	
Treatment	*p*IC_{50}	P	*p*IC_{50}	P	*p*IC_{50}	P	*p*IC_{50}	P
Vehicle	9.3 ± 0.1	N.A.	9.6 ± 0.1	N.A.	8.2 ± 0.1	N.A.	6.6 ± 0.7	N.A.
AMD3100	9.3 ± 0.1	0.99	9.6 ± 0.1	0.93	8.1 ± 0.3	0.95	6.3 ± 1.3	0.95
IT1t	**10.1 ± 0.1**	****	**10.0 ± 0.1**	**	**8.9 ± 0.1**	*	9.7 ± 0.4	0.08
VUN401	**9.7 ± 0.2**	**	N.D.	N.D.	N.D.	N.D.	N.D.	N.D.

Table S3. Effects of CXCR4 ligands on venetoclax potency in different MCL and CLL cell lines in a FACS viability readout. Data are the pooled mean ± SEM of at least three independent experiments, each performed in triplicate. Significant differences (P < 0.05) compared to vehicle condition are indicated in bold, according to a one-way ANOVA followed by Dunnett's post hoc test. * P < 0.05, ** P < 0.01.

	Z-138		Maver-1		Jeko-1	
Treatment	pIC_{50}	P	pIC_{50}	P	pIC_{50}	P
Vehicle	8.5 ± 0.6	N.A.	9.3 ± 0.3	N.A.	8.8 ± 0.6	N.A.
IT1t	**9.7 ± 0.4**	*	9.6 ± 0.3	0.1	**9.8 ± 0.5**	*
AMD070	**8.8 ± 0.7**	**	9.5 ± 0.5	0.2	9.0 ± 0.7	0.3
TG-0054	8.3 ± 1	0.3	9.2 ± 0.3	0.1	8.9 ± 0.4	0.8
AMD3100	8.3 ± 0.9	0.3	9.2 ± 0.4	0.3	8.9 ± 0.5	0.4
VUN401	8.8 ± 0.3	0.1	N.D.	N.D.	N.D.	N.D.

Table S4. Patient information table. Information about the used CLL and MCL patient samples in this study.

Malignancy	Sample	Sample date	Age	Gender	IGHV	FISH/mutations	Treatment
CLL	1961	16-06-2017	84	M	Mutated	Trisomy 12	Prednisone
	2148	19-03-2018	81	M	Mutated	del(13q14), TP53 mutation (VAF 1%)	none
	1576	11-12-2014	88	F	Mutated	Not performed	none
	2094	23-01-2018	64	F	Unmutated	trisomy 12, del(4p15.2-p15.1), TP53 WT	none
	2748	18-11-2019	65	F	Unmutated	trisomy 12, del(4p15.2-p15.1), TP53 WT	none
	2747	14-11-2019	63	M	Unmutated	Absence del11q, absence del17p, TP53 WT	none
	664	12-06-2008	85	M	Mutated	del(13q14) 58%, del(14q32)(IGH) 9%	none
	50	15-10-2004	64	F	Mutated	Not performed	none
MCL	2257	14-06-2018	57	M	ND	T(11;14) 80%, del(13q14) (loss of DLEU2/MIR15A/MIR16-1 and RB1 locus), del(17p13.1) (TP53), del(2q33.2-q34), dup(5q33.2-q34), dup(8p23.1-p22), del(9p24.1-p21.3), del(10p15.3-p13), 13q12.11-q13.3), chromotrypsis can chr. 14, dup(16q21-q22), dup(22q12.3-q13.2)	2015: Acerta Btk inh. 20-06-2018: R Benda.
	No sample number available, only date	19-07-2016	68	M	ND	t (11;14) in 78% cells, complex karyotype with gain MYC.	Rasburicase & levocetirizine. Patient left ACERTA trial (acelabrutinib) just before sample. Had 6 cycles of acalabrutinib with comple remission.
	No sample number available, only date	11-07-2014	79	F	ND	T(11;14)(q13;q32) 20%, cycline d1 translocatie	1st cycle Benda 17-07-2014.

SI references

1. L. A. Goldman, E. C. Cutrone, S. V. Kotenko, C. D. Krause, J. A. Langer, Modifications of vectors pEF-BOS, pcDNA1 and pcDNA3 result in improved convenience and expression. *BioTechniques* **21**, 1013-1015 (1996).
2. J. S. Paradis *et al.*, Computationally designed GPCR quaternary structures bias signaling pathway activation. *Nat Commun* **13**, 6826 (2022).
3. A. O. Watts *et al.*, Identification and profiling of CXCR3-CXCR4 chemokine receptor heteromer complexes. *Br. J. Pharmacol.* **168**, 1662-1674 (2013).
4. J. van den Bor *et al.*, NanoB(2) to monitor interactions of ligands with membrane proteins by combining nanobodies and NanoBRET. *Cell Rep Methods* **3**, 100422 (2023).
5. A. Isbilir *et al.*, Advanced fluorescence microscopy reveals disruption of dynamic CXCR4 dimerization by subpocket-specific inverse agonists. *Proc Natl Acad Sci U S A* **117**, 29144-29154 (2020).
6. R. H. de Wit *et al.*, Human cytomegalovirus encoded chemokine receptor US28 activates the HIF-1α/PKM2 axis in glioblastoma cells. *Oncotarget* **7**, 67966-67985 (2016).
7. J. R. van Senten *et al.*, The human cytomegalovirus-encoded G protein-coupled receptor UL33 exhibits oncomodulatory properties. *J. Biol. Chem.*, (2019).
8. T. W. M. De Groof *et al.*, Selective targeting of ligand-dependent and -independent signaling by GPCR conformation-specific anti-US28 intrabodies. *Nat Commun* **12**, 4357 (2021).
9. D. Y. Hallaert *et al.*, c-Abl kinase inhibitors overcome CD40-mediated drug resistance in CLL: implications for therapeutic targeting of chemoresistant niches. *Blood* **112**, 5141-5149 (2008).
10. H. C. Lantermans *et al.*, Identification of the SRC-family tyrosine kinase HCK as a therapeutic target in mantle cell lymphoma. *Leukemia* **35**, 881-886 (2021).
11. A. Van Hout *et al.*, CXCR4-targeting nanobodies differentially inhibit CXCR4 function and HIV entry. *Biochem. Pharmacol.* **158**, 402-412 (2018).
12. M. Godar *et al.*, Dual anti-idiotypic purification of a novel, native-format biparatopic anti-MET antibody with improved in vitro and in vivo efficacy. *Sci Rep* **6**, 31621 (2016).
13. S. M. Anbuhl *et al.*, Multivalent CXCR4-targeting nanobody formats differently affect affinity, receptor clustering, and antagonism. *Biochem. Pharmacol.* **227**, 116457 (2024).
14. W. Ren *et al.*, One-Step Ultrasensitive Bioluminescent Enzyme Immunoassay Based on Nanobody/Nanoluciferase Fusion for Detection of Aflatoxin B(1) in Cereal. *J. Agric. Food Chem.* **67**, 5221-5229 (2019).
15. R. Heukers *et al.*, The constitutive activity of the virally encoded chemokine receptor US28 accelerates glioblastoma growth. *Oncogene*, **37**, 4110-4121 (2018).
16. A. Chazeau, E. A. Katrukha, C. C. Hoogenraad, L. C. Kapitein, Studying neuronal microtubule organization and microtubule-associated proteins using single molecule localization microscopy. *Methods Cell Biol* **131**, 127-149 (2016).
17. A. D. Edelstein *et al.*, Advanced methods of microscope control using muManager software. *J Biol Methods* **1**, e10 (2014).
18. L. Andronov, I. Orlov, Y. Lutz, J. L. Vonesch, B. P. Klaholz, ClusterViSu, a method for clustering of protein complexes by Voronoi tessellation in super-resolution microscopy. *Sci Rep* **6**, 24084 (2016).
19. M. V. Haselager *et al.*, In Vitro 3D Spheroid Culture System Displays Sustained T Cell-dependent CLL Proliferation and Survival. *Hemasphere* **7**, e938 (2023).